This is the accepted manuscript (postprint) of the following article:
M. Shahrouzifar, E. Salahinejad, E. Sharifi, *Co-incorporation of strontium and fluorine into diopside scaffolds: bioactivity, biodegradation and cytocompatibility evaluations*, Materials Science and Engineering: C, 103 (2019) 109752.
https://doi.org/10.1016/j.msec.2019.109752

Co-incorporation of strontium and fluorine into diopside scaffolds: bioactivity, biodegradation and cytocompatibility evaluations

M.R. Shahrouzifar [a], E. Salahinejad [a,*] E. Sharifi [b]

[a] Faculty of Materials Science and Engineering, K. N. Toosi University of Technology, Tehran, Iran

[b] Department of Tissue Engineering and Biomaterials, School of Advanced Medical Sciences and Technologies, Hamadan University of Medical Sciences, Hamadan, Iran

Abstract

This study focuses on the effect of Sr-, F-, and their co-doping on the structure, biodegradation, bioactivity and cytocompatibility of diopside-based scaffolds, using X-ray diffraction, Raman spectroscopy, field-emission scanning electron microscopy, Archimedes densitometry, inductively coupled plasma spectroscopy, pH-metry, and cell MTT assay. The structural characterization of the scaffolds confirmed the successful incorporation of the dopants into the ceramic. In addition, all the doped scaffolds presented higher apatite-forming ability levels in comparison to the undoped one, where the highest and the least impact of doping on bioactivity belonged to F- and co-doping, respectively. It was found that the biodegradation difference of the scaffolds in terms of principal ions and the chance of F-incorporation into precipitated apatite determine the bioactivity difference of the samples. Osteoblast-like MG-63 cells exhibited the highest and lowest compatibility to the Sr-doped and co-doped scaffolds, respectively. In summary, F- and Sr-doping offered the highest

* Corresponding Author: Email Address: <salahinejad@kntu.ac.ir>

This is the accepted manuscript (postprint) of the following article:
M. Shahrouzifar, E. Salahinejad, E. Sharifi, *Co-incorporation of strontium and fluorine into diopside scaffolds: bioactivity, biodegradation and cytocompatibility evaluations*, Materials Science and Engineering: C, 103 (2019) 109752.
https://doi.org/10.1016/j.msec.2019.109752

bioactivity and cytocompatibility, respectively, whereas co-doping presented the weakest behaviors comparatively.

Keywords: Tissue Engineering Scaffolds; Diopside; Doping; Bioactivity; Cytocompatibility

1. Introduction

In the past decades, due to the increase of the world's elderly population, age-related diseases like osteoporosis and bone fragility have been increased. Hence, new biomaterials, substituting for damaged tissues and stimulating repair and regeneration mechanisms, are required. In this regard, three-dimensional (3D) porous scaffolds can be designed for the reconstruction and repair of damaged tissues. For bone tissue regeneration, biomaterials like Mg-containing bioactive silicates are of great interest, due to the possession of proper mechanical properties, bioactivity, and biocompatibility [1-5]. Akermanite, Bredigite, Forsterite, Merwinite, Monticellite, Proto-enstatite, and Pyroxene exemplify Mg-containing silicates. Another member of these bioceramics is Diopside ($CaMgSi_2O_6$) which can be utilized in tissue engineering applications, with the typical advantages of suitable mechanical properties, biocompatibility, cell adhesion, proliferation, and differentiation [6-8].

The presence of the high level of magnesium in diopside stimulates the formation of new bone and increases the adhesion and stability of bone cells [9, 10]. However, the excessive amount of magnesium retards the apatite-forming ability of bioceramics [11]. Indeed, a high release level of Mg ions from Mg-containing ceramics into the SBF impedes the apatite-forming ability of the bioceramics [12]. Because of this, diopside does not demonstrate high bioactivity [2, 6, 13-16], where the rising demand for the usage of this bioceramic in the bone tissue engineering field needs more improvements in this property.

This is the accepted manuscript (postprint) of the following article:
M. Shahrouzifar, E. Salahinejad, E. Sharifi, *Co-incorporation of strontium and fluorine into diopside scaffolds: bioactivity, biodegradation and cytocompatibility evaluations*, Materials Science and Engineering: C, 103 (2019) 109752.
https://doi.org/10.1016/j.msec.2019.109752

To improve the apatite-forming ability of diopside, doping of suitable ions which can limit Mg liberation can have a positive effect. On the one hand, strontium doping into several bioceramics has been associated with lowering the release rate of ionic constituents [17-21]. On the other hand, fluoride has been reported to boost the precipitation of apatite on $2SiO_2$-MgO-CaO bioactive glass and crystalline diopside [22-24]. Nonetheless, there are optimal incorporation levels of both dopants to meet the best bioactivity and biocompatibility of bioceramics including diopside [24, 25]. The hypothesis of this work, on which no studies have been reported to our knowledge, is that co-doping of fluoride and strontium into diopside may improve the biological behaviors of this bioceramic more than the mono-doped cases.

2. Experimental procedure

2.1. Materials used

In the current study, calcium chloride ($CaCl_2$, Merck, > 98%), magnesium chloride ($MgCl_2$, Merck, > 98%), silicon tetrachloride ($SiCl_4$, Merck, > 99%), dry ethanol (C_2H_5OH, Merck, > 99%), and aqueous ammonia solution (NH_4OH, Merck, 25%) were used to synthesize diopside powders. Also, strontium chloride ($SrCl_2$, Merck, > 98%) and magnesium fluoride (MgF_2, Alfa Aesar, > 99%) were utilized as the sources of doping agents.

2.2. Fabrication of scaffolds

Undoped and doped diopside powders were synthesized by coprecipitation. For pure diopside, a same molar of $CaCl_2$ and $MgCl_2$ were dissolved in dry ethanol in an ice-water bath. After thorough dissolution, the proper content of $SiCl_4$ (giving the cationic

This is the accepted manuscript (postprint) of the following article:
M. Shahrouzifar, E. Salahinejad, E. Sharifi, *Co-incorporation of strontium and fluorine into diopside scaffolds: bioactivity, biodegradation and cytocompatibility evaluations*, Materials Science and Engineering: C, 103 (2019) 109752.
https://doi.org/10.1016/j.msec.2019.109752

stoichiometry of diopside) was added to the solution. For precipitation, ammonium hydroxide solution was added until pH reached to 10. After drying the obtained products at 100 °C, they were grounded and calcined at 700 °. The synthesis of the doped diopside powders was similar to the above procedure, with the difference that in case of Sr-doping , $SrCl_2$ was substituted for $CaCl_2$ at 2 mol%, yielding $Ca_{0.98}Sr_{0.02}MgSi_2O_6$. Additionally, 1 mol% fluoride was incorporated into diopside via the addition of MgF_2 before the usage of the ammonia solution, where the same molar amount of MgF_2 was subtracted from the molar content of $MgCl_2$ used to keep the molar ratio of Ca:Mg:Si=1:1:2 in diopside. For co-doping into diopside, $CaCl_2$, $MgCl_2$, $SiCl_4$, $SrCl_2$ and MgF_2 were employed at the molar ratio of 0.98:0.95:2:0.02:0.05, giving the composition of $Ca_{0.98}Sr_{0.02}MgSi_2O_{5.95}F_{0.1}$.

A sacrificial template method using a polyurethane foam with the open and interconnected porosity of approximately 25 pores per inch was utilized to fabricate scaffolds from the calcined powders. Briefly, the undoped and doped powders were separately suspended in 6 wt% polyvinyl alcohol aqueous solution under stirring and sonication. Cubic polyurethane foams were immersed in well-dispersed slurries and compressed for the penetration of the slurry into pores. In order to blow away the remained slurry and prevent blocking the pores, the immersed scaffolds underwent a compressed air flow. After drying the foams with a slightly warm flow, they were experienced a heat-treatment cycle as follows: firing at 400 °C for the decomposition of the polyurethane foam template and then sintering at 1200 °C at a heating rate of 5 °C/m.

2.3. Structural characterization of scaffolds

This is the accepted manuscript (postprint) of the following article:
M. Shahrouzifar, E. Salahinejad, E. Sharifi, *Co-incorporation of strontium and fluorine into diopside scaffolds: bioactivity, biodegradation and cytocompatibility evaluations*, Materials Science and Engineering: C, 103 (2019) 109752.
https://doi.org/10.1016/j.msec.2019.109752

X-ray diffraction (XRD, PANalytical, X'pert Pro MPD, Cu-Kα radiation, step size: 0.03°, step time: 3 s) and Raman spectroscopy (Handheld Raman analyzer, Rigaku, wavenumber range: 200-2000 cm^{-1}) were used for phase characterization and identification of bonding formed in the samples. Also, the sintered scaffolds were observed by field-emission scanning electron microscopy (FESEM, MIRA3TESCAN-XMU, accelerating voltage: 15 kV). The water Archimedes method was also used to measure the porosity level of the scaffolds [26].

2.4. Apatite-forming ability and degradation of scaffolds

The sintered scaffolds were immersed in the simulated body fluid (SBF) for 7 days at 37 °C. The ratio of the solution volume to the scaffold mass was equal to 200 $ml.g^{-1}$. The scaffolds were then rinsed with water and dried at room temperature for 3 days. Afterwards, they were assessed by FESEM equipped with energy-dispersive X-ray spectroscopy (EDS) and Raman spectroscopy. The concentration of principal ions in the SBF was measured by inductively coupled plasma spectroscopy (ICP-OES, OES-730, Varian) before and after contact with the scaffolds. The pH value of the SBF during immersion was also reported as the averages of several measurements.

2.5. Cytocompatibility

2×10^4 of human osteosarcoma MG-63 cells in Dulbecco's modified Eagle's medium-low glucose (Gibco, USA) supplemented with 10% fetal bovine serum (Gibco, USA) and 1% penicillin-stroptomycine (Gibco, USA) were seeded onto the sterilized scaffolds (6×6×6 mm^3) which were put individually in a 24-well plate. The scaffold-free cell-loaded medium

This is the accepted manuscript (postprint) of the following article:
M. Shahrouzifar, E. Salahinejad, E. Sharifi, *Co-incorporation of strontium and fluorine into diopside scaffolds: bioactivity, biodegradation and cytocompatibility evaluations*, Materials Science and Engineering: C, 103 (2019) 109752.
https://doi.org/10.1016/j.msec.2019.109752

was also used as the control. After the plates were left in an incubator for 24, 48, and 72 h at 37 °C in a humidified atmosphere of 95% air and 5% CO_2, 50 µl of the MTT solution was poured to the well plates and they then were transferred to the incubator for 3 h. Afterwards, the culture medium was removed from the wells and 500 µl of dimethyl sulfoxide (DMSO) solution was added to each well. 250 µl of formazan crystals dissolved in the DMSO solution were transferred to a 96-well plate for measuring the optical density at 570 nm using a Stat Fax 2100 microplate reader. The cytocompatibility and cell viability data were analyzed using the one-way analysis of variance (ANOVA) with a p-value <0.05 as a statistically significance level for three repetitions.

3. Results and discussion

3.1. Structural characterization of scaffolds

Fig. 1 shows the XRD patterns of the F- and co-doped powders calcined with the heat procedure of scaffolding (those of the undoped and Sr-doped samples have been provided in Ref. [25]). As can be seen, the patterns merely indicate the characteristic peaks of diopside (Ref. code: 00‑017-0318). This suggests that the incorporation of F^- and Sr^{2+} at this level into diopside, in all of the mono- and co-doped cases, does not result in the formation of any secondary phases.

The Raman spectroscopic analysis of bonding was conducted on the fabricated scaffolds before immersion in the SBF (Fig. 2). In the Raman spectrum of pure diopside, peaks of 1016 and 848 cm^{-1} are assigned to the non-bridging stretching modes of the Si-O bonding. The bridging stretching vibration of Si-O and the bending mode of O-Si-O are attributed to peaks of 664 and 507 cm^{-1}, respectively [27]. The wavenumber range of 451-489

This is the accepted manuscript (postprint) of the following article:
M. Shahrouzifar, E. Salahinejad, E. Sharifi, *Co-incorporation of strontium and fluorine into diopside scaffolds: bioactivity, biodegradation and cytocompatibility evaluations*, Materials Science and Engineering: C, 103 (2019) 109752.
https://doi.org/10.1016/j.msec.2019.109752

cm^{-1} contains the rocking vibrations of the siloxane (Si-O-Si) functional group [28]. The stretching modes of Mg-O and Ca-O are also pointed out from peaks of 393 and 364 cm^{-1}, respectively. In addition, peaks of 325 and 236 cm^{-1} can be attributed to the stretching modes of M-O, where M is Ca or Mg [29, 30]. Sr-doping leads to increases in the intensity of the peaks appearing in the range of 200-591 cm^{-1}, in comparison to the Raman spectrum of pure diopside. Nonetheless, the other vibrational peaks exhibit decreases in intensity as a result of Sr-doping. In this sample, peak shifts of 8-10 cm^{-1} toward lower wavenumbers are also detected for the non-bridging stretching modes of Si-O and Mg-O, giving peaks at 1008 and 383 cm^{-1}. These variations in the Raman spectra as a result of Sr-doping, as evidences for the incorporation of strontium into diopside, on the one hand, are attributed to the larger ionic size of strontium compared to calcium. Because by the incorporation of larger-sized cations into pyroxenes, including diopside, the average band distance of the bridging and non-bridging Si-O is increased and decreased, respectively [31, 32]. On the other hand, the higher polarizability of Sr-O than Ca-O [33] explains the increase in the Raman intensity of the broad peak in the range of 200-591 cm^{-1} due to the partial substitution of Sr for Ca. Compared to Sr, F-doping results in more significant variations in the Raman spectra of diopside. The peak of 1000 cm^{-1} is related to the non-bridging stretching mode of Si-O, i.e. a peak shift of 16 cm^{-1}. Also, the bridging stretching vibration of Si-O was shifted to the wavenumber of 655 cm^{-1} with a significant decrease in intensity. The appearance of new peaks, including 1049 and 857 (the non-bridging stretching vibrations of Si-O [27]), 655 (the bridging stretching vibrations of Si-O [29, 34]), 563 (the bending vibrations of O-Si-O [27, 35]), 432 (five-fold rings of Si-O-Si [27, 35]), and 451-489 cm^{-1} (the rocking vibrations of Si-O-Si [28]), is additionally a typical consequence of F-doping. Due to F-doping, the stretching

This is the accepted manuscript (postprint) of the following article:
M. Shahrouzifar, E. Salahinejad, E. Sharifi, *Co-incorporation of strontium and fluorine into diopside scaffolds: bioactivity, biodegradation and cytocompatibility evaluations*, Materials Science and Engineering: C, 103 (2019) 109752.
https://doi.org/10.1016/j.msec.2019.109752

vibration of Mg-O is also shifted to 383 cm^{-1}; furthermore, another additional adsorption band appears at 797 cm^{-1} which corresponds to Si-F [36]. These significant variations are attributed to the higher bond strength of Si-F than Si-O, which dictates a change in the charge distribution on Si-O when a number of O-Si-O is converted to O-Si-F. The great ability of F in electron dragging from O enhances the covalent character of the Si-O bonds, thereby changes the bond polarizability and Raman vibrations. In the Raman spectrum of the co-doped scaffold, the peak shift for the stretching vibration of Mg-O to 383 cm^{-1} and a new peak at 797 cm^{-1} corresponding to Si-F [36] are recognized. Thus, the Raman spectroscopy infers that:

a) The diopside structure has been formed in the sintered scaffolds, which is realized from the detected functional groups of this phase.

b) The doping agents have been successfully incorporated in the samples, which is speculated from the variations detected in the peak intensity and wavenumber in the doped samples, in comparison to the pure samples.

The FESEM micrographs of the undoped diopside scaffold are shown in Fig. 3. The scaffolds contain a wealth of open and interconnected pores, with a pore size range of about 300-700 μm and a median pore diameter of almost 500 μm. The porosity percentage of the scaffolds was measured to be about 90-92% by the Archimedes densitometric method, which is anticipated to be desirable for tissue ingrowth, cell penetration, vascularization, and nutrient transport [37, 38]. According to the high-magnification FESEM micrograph of the scaffolds, the pore walls (struts) are porous and contain irregular-shaped particles of 50-500 nm in size. It is noteworthy that these nanometer-to-micron sized pores and particles are useful for bioactivity.

This is the accepted manuscript (postprint) of the following article:
M. Shahrouzifar, E. Salahinejad, E. Sharifi, *Co-incorporation of strontium and fluorine into diopside scaffolds: bioactivity, biodegradation and cytocompatibility evaluations*, Materials Science and Engineering: C, 103 (2019) 109752.
https://doi.org/10.1016/j.msec.2019.109752

3.2. Apatite-forming ability and biodegradation of scaffolds

Fig. 4 shows the FESEM micrographs of the scaffolds after 7 days of incubation in the SBF. Based on the taken micrographs, the *in vitro* apatite-forming ability of the samples is comparatively enhanced in the following order: pure, co-doped, Sr-doped, and F-doped diopside scaffolds. Morphologically, apatite spheres were formed on the surface of the F-doped and Sr-doped scaffolds, whereas some sparse plates of apatite were observed on that of the pure diopside scaffold. In contrast, the co-doped scaffold reveals a combination of spheres and plates of apatite. Quantitatively, the mean diameter of the apatite spheres on the F-doped and Sr-doped scaffolds is 2.29 and 1.64 μm, respectively, whereas the average thickness of the apatite plates on the pure and co-doped scaffolds is 38.4 and 45.4 nm, respectively. All of the formed apatites exhibit a leaf-like morphology, according to the high-magnification micrographs.

The Raman spectra of the samples after immersion in the SBF are depicted in Fig. 5. In comparison to the spectra before immersion (Fig. 2), for the pure diopside scaffold, two new peaks are emerged at the wavenumbers of 958 and 1081 cm^{-1}, which can be assigned to the stretching vibration modes of P-O (v_3) and P-O (v_1) in the phosphate (PO_4^{-3}) group, respectively [39, 40]. Also, the peak of 1081 cm^{-1} is associated to the carbonate (CO_3^{-2}) functional group [41]. The decrease in the intensity of the two peaks at 848 and 1016 cm^{-1} (related to the bridging stretching mode of Si-O) after soaking in the SBF can be attributed to the formation of the silanol (Si-OH) functional group due to the release of Ca^{2+} and Mg^{2+} [42]. Concerning the Sr-doped sample, peaks of 433 and 591 cm^{-1} are assigned to the bending vibration mode of O-P-O (v_2) and (v_4) in the phosphate group of hydroxyapatite, respectively

This is the accepted manuscript (postprint) of the following article:
M. Shahrouzifar, E. Salahinejad, E. Sharifi, *Co-incorporation of strontium and fluorine into diopside scaffolds: bioactivity, biodegradation and cytocompatibility evaluations*, Materials Science and Engineering: C, 103 (2019) 109752.
https://doi.org/10.1016/j.msec.2019.109752

[39, 40, 43]. The typical peak of 983 cm^{-1} corresponds to the stretching vibration of P-O (v_1) in the phosphate group [39, 40]. Additionally, peaks of 1049, 1089 and 1113 cm^{-1} are attributed to the stretching vibration of P-O (v_3) in the phosphate groups [43, 44]. The peaks of 691 and 1073 cm^{-1} are also related to the vibrations of C-O (v_4) and (v_1) in the carbonate group [41]. In the Raman spectrum of the F-doped samples, peaks of 403 and 432 cm^{-1} correspond to the bending vibration mode of O-P-O (v_2) in the phosphate group [39, 40, 43]. The bending vibrations of O-P-O (v_4) and O-C-O (v_4) are also observed at the wavenumbers of 618 and 713 cm^{-1}, respectively [40, 41, 43]. Two peaks of 1008 and 1081 cm^{-1} are respectively indicative of the stretching vibration of P-O (v_1) and C-O (v_1) in the hydrogen phosphate (HPO_4^{2-}) and carbonate groups [39-41, 44, 45]. The peak formed at the wavenumber of 1121 cm^{-1} is attributed to the stretching vibration of P-O (v_3) in the functional group of hydrogen phosphate [40]. Three peaks of 1412, 1452 and 1488 cm^{-1} are also related to C-O (v_3) in the carbonate functional group of carbonate fluorapatite [41]. In the Raman spectrum of the immersed co-doped scaffold, the bending vibration of O-P-O (v_2) in the hydrogen phosphate group is observed at 354 and 412 cm^{-1}. Also, the wavenumbers of 432 and 451cm^{-1} are related to the bending vibration of O-P-O (v_2) in phosphate group. The wavenumbers of 526 and 618 cm^{-1} are assigned to the bending vibration of O-P-O (v_4) in the phosphate group [39, 40, 43, 44]. The stretching vibration of P-O (v_1) in the phosphate group is also observed at 958 cm^{-1}. Three peaks at 691, 709 and 866 cm^{-1} correspond to C-O (v_4) in the carbonate functional group. Peaks of 1073 and 1459 cm^{-1} are also attributed to C-O (v_1) and C-O (v_3), respectively, in the carbonate functional group [41]. The relatively weak peak at 637 cm^{-1} is indicative of the hydroxyl (OH^-) group. The following conclusions can be drawn from the Raman spectroscopic analyses:

This is the accepted manuscript (postprint) of the following article:
M. Shahrouzifar, E. Salahinejad, E. Sharifi, *Co-incorporation of strontium and fluorine into diopside scaffolds: bioactivity, biodegradation and cytocompatibility evaluations*, Materials Science and Engineering: C, 103 (2019) 109752.
https://doi.org/10.1016/j.msec.2019.109752

i) The precipitates formed on the scaffold surfaces due to incubation in the SBF, as characterized by the FESEM analysis (Fig. 4), are hydroxycarbonate apatite ($Ca_5(PO_4)_{3-x}(CO_3)_xOH$), showing their *in vitro* bioactivity.

ii) Comparing the variations in the spectra before and after soaking in the SBF, the apatite-forming ability ranking of the scaffolds realized from the FESEM observations is verified, i.e. F-doped > Sr-doped > co-doped > undoped diopside.

Fig. 6 indicates the ICP concentration of Ca, Si, Mg, Sr, F and P ions in the SBF after 7 days of contact with the scaffolds. In comparison to the fresh SBF, the concentration of Ca is increased for all the immersed scaffolds. This variation is a sign of biodegradation and vital for apatite precipitation through making a supersaturated microenvironment. In other words, the final amount of this ion in the SBF is determined by a compromise of apatite precipitation and matrix dissolution. Since this ion exists in both the fresh SBF and diopside, the variations in its concentration after immersion cannot be used as a criterion for the evaluation of the apatite-forming ability level. For all the immersed scaffolds, the concentration of Si and Mg is also increased, due to dissolution of the scaffolds. The lowest level of Si in the SBF is detected for the F-doped diopside scaffold, which is attributed to the higher electronegativity of F than O and the stronger bond strength Si-F than Si-O [24, 46]. The larger radius of Sr^{2+} in comparison to Ca^{2+} also explains the limited release of Si from the Sr-doped scaffold [18, 47]. The higher level of Si degradation for the co-doped sample is owing to the fact that the simultaneous use of F and Sr negates the inhibitory effect of each species. Sr is more electropositive than Ca and Mg; therefore, the bond strength of Sr-F is higher than Mg-F and Ca-F. The lower release amounts of Sr and F ions from the co-doped scaffold with respect to the release of Sr and F ions from the Sr- and F-doped scaffolds, respectively, verifies the high

This is the accepted manuscript (postprint) of the following article:
M. Shahrouzifar, E. Salahinejad, E. Sharifi, *Co-incorporation of strontium and fluorine into diopside scaffolds: bioactivity, biodegradation and cytocompatibility evaluations*, Materials Science and Engineering: C, 103 (2019) 109752.
https://doi.org/10.1016/j.msec.2019.109752

bond strength of Sr-F. It dictates a change in the charge distribution on the Si-O bond in the ≡Si-O-Sr-F group and facilitates the release of Si ions in the co-doped scaffold in comparison to the Sr-and F-doped ones. Since the fresh SBF has no Si ions, the concentration of Si ions in the SBF after immersion was employed as a criterion for measuring the weight loss of the scaffolds, using the following equation:

$$d = (C_{Si} \times V_S) / m_{Si} \times 100 \quad (1)$$

where C_{Si}, V_S and m_{Si} represent the concentration of Si in the SBF, the volume of the SBF (ml) and the Si content (mg) of the samples immersed in the SBF, respectively. The weight loss of the pure, Sr-, F-, and co-doped diopside scaffolds after immersion in the SBF was calculated to be 4.17, 3.33, 3.26, and 3.57 %, respectively. That is, all the doped scaffolds show lower weight losses compared to the pure one. Also, the F-doped scaffold possesses the least level of degradation. The trend and reasons of the variations in the concentration of Mg of the SBFs resemble Si. More importantly, because of the lack of P in the scaffolds and the direct consumption of this ion from the SBF toward apatite precipitation, the final value of this species in the SBF is regarded as a criterion to compare apatite-forming ability. In agreement with the FESEM and Raman analyses, the ICP analysis of P also verified that the bioactivity of the scaffolds ranks as the F-doped > Sr-doped> co-doped> undoped samples.

To correlate the bioactivity and bioresorbability of the scaffolds, the pH variations of the SBF in contact with the immersed scaffolds was also measured (Fig. 7). Before immersion, the fresh SBF had pH=7.4. After contact with all scaffolds, pH is enhanced until the 4th and 5th day, but it then faces a decrease until the 7th day. This enhancement is indicative of the decrease in the concentration of H^+ or H_3O^+ in the SBF, due to exchanges with Ca^{2+}, Mg^{2+}, and Sr^{2+}released from the scaffolds as detected by the ICP analysis. The

This is the accepted manuscript (postprint) of the following article:
M. Shahrouzifar, E. Salahinejad, E. Sharifi, *Co-incorporation of strontium and fluorine into diopside scaffolds: bioactivity, biodegradation and cytocompatibility evaluations*, Materials Science and Engineering: C, 103 (2019) 109752.
https://doi.org/10.1016/j.msec.2019.109752

consequent decrease in pH is due to the domination of the formation of hydroxyapatite (realized by the FESEM and Raman analyses) consuming OH^- in the SBF. During this period of incubation, the pH values mainly rank as: undoped > co-doped> F-doped> Sr-doped. Regarding Sr, the presence of this species in bioceramics indicates different contributions to biodegradation and pH variations in the SBF. As an example, Zhu et al. [21] investigated the effect of Sr substitution for Ca in amorphous $CaSiO_3$. They showed the pH value of the SBF is decreased by increasing the percentage of Sr. In contrast, Zreiqat et al. [48] found an increasing trend of pH when the SBF is exposed to Hardystonite ($Ca_2ZnSi_2O_7$) with the 5 mol% replacement of Ca by Sr. For the F-doped sample, the less pronounced upswing of pH in comparison to pure diopside up to the 5th day of soaking is related to, on the one hand, the minor liberation of Ca^{2+} and Mg^{2+}, limiting the consumption of H^+ (H_3O^+). On the other hand, the incorporation of fluoride in diopside causes the formation of ≡Si-F, ≡Si-O-Ca-F and ≡Si-O-Mg-F bonds. Considering the same electrical charge of fluoride and hydroxyl anion, OH^- can be directly replaced with F^-, creating ≡Si-OH, ≡Si-O-Ca-OH and ≡Si-O-Mg-OH bonds in turn. This consumption source of hydroxyl buffers the early increase of pH for the F-doped sample. The higher value of pH for the co-doped sample, with respect to Sr- and F-doped diopside, is also attributed to the more degradation of the cations and the lower release of F^- from this sample toward the SBF, as realized by the ICP analysis.

Based on the FESEM, Raman, and ICP analyses, the apatite-forming ability of the samples was ranked as: F-doped > Sr-doped> co-doped> undoped samples. The highest apatite-forming ability rank of the F-doped sample is attributed to fluoride incorporation into apatite formed on its surface, because this ion enhances the stability of apatite against dissolution [49-52]. The incorporation of fluoride is inferred from the carbonate vibrations of

This is the accepted manuscript (postprint) of the following article:
M. Shahrouzifar, E. Salahinejad, E. Sharifi, *Co-incorporation of strontium and fluorine into diopside scaffolds: bioactivity, biodegradation and cytocompatibility evaluations*, Materials Science and Engineering: C, 103 (2019) 109752.
https://doi.org/10.1016/j.msec.2019.109752

1412, 1452 and 1488 cm^{-1} associated with fluorocarbonate apatite in the Raman spectrum of the F-doped sample after immersion in the SBF (Fig. 5). Also, the exchange of F^- released from the sample with OH^- of the SBF increases the level of surface silanol (Si-OH) functional groups which play an essential role in the apatite nucleation and bioactivity [53]. The comparative apatite-forming ability rank of the co-doped sample can be explained by comparing the degradation rate of this sample with the other samples (Fig. 6). In comparison to undoped diopside, as well as the positive contributions of F^- and Sr^{2+}, the less release of Mg^{2+} from the co-doped sample is beneficial for bioactivity, because Mg^{2+} ions retards the formation of calcium phosphate. This is due to the competitive bonding between magnesium, rather than calcium, and phosphorus ions on the bioceramic surface [54]. In comparison to F-doped diopside, the lower release of F^- from co-doped diopside contributes to the lower incorporation of this anion into apatite, as realized from the reduced intensity of the carbonate peak at 1459 cm^{-1} (related to fluorocarbonate apatite). This results in a decrease in the dissolution resistant of the formed apatite and thereby in bioactivity compared to the F-doped sample. Also, the decrease in the release of fluoride brings about a reduction in the replacement with hydroxyl anions and consequently in the formation of surface Si-OH groups. The lower bioactivity of the co-doped sample with respect to the F-doped one suggests that the explained contribution of fluoride prevails over the positive contribution of Sr^{2+}. Finally, the lower bioactivity of the co-doped sample compared to the Sr-doped sample is attributed to the lower release of Sr from this sample. The positive role of Sr^{2+} in bioactivity can be attributed to its exchange with H^+ or H_3O^+ and hence the creation of silanol functional groups. That is, the contribution of Sr^{2+} prevails over that of F^-, in the bioactivity comparison of the Sr- and co-doped samples.

This is the accepted manuscript (postprint) of the following article:
M. Shahrouzifar, E. Salahinejad, E. Sharifi, *Co-incorporation of strontium and fluorine into diopside scaffolds: bioactivity, biodegradation and cytocompatibility evaluations*, Materials Science and Engineering: C, 103 (2019) 109752.
https://doi.org/10.1016/j.msec.2019.109752

3.3. Cytocompatibility of scaffolds

In order to evaluate cytotoxicity induced by ions released from the scaffolds, the MTT assay was used after the MG-63 cell cultures on the samples for 24, 48, and 72 h (Fig. 8). The increase in the number of viable cells (optical density values) from 24 h to 72 h is indicative of effective cell proliferation on the surfaces. Considering the significance level of $p<0.05$, the cytocompatibility of the samples is almost equivalent at the culture time of 24 h. However, for the culture periods of 48 and 72 h, the number of viable cells on the F- and co-doped samples is less than the pure and Sr-doped scaffolds. That is, Sr-doping is beneficial to cytocompatibility with respect to osteoblast-like MG-63 cells, which is compatible with the literature [18, 48, 55-60]. In contrast, F-doping at this level, despite the most positive effect on bioactivity in comparison to the other samples (Figs. 4, 5, and 6), lowers the cytocompatibility of diopside, so that even Sr-doping is not able to compensate this deterioration in the case of co-doping. Regarding the reduced cytocompatibility of the co-doped sample, as well as the negative effect of fluoride, the decrease in the level of advantageous Sr ions released into the medium (Fig. 6) is noticeable.

4. Conclusions

In this work, the structure (including bonding, and porosity), apatite-forming ability, biodegradation, and cytocompatibility of highly porous pure, Sr-doped, F-doped and co-doped diopside scaffolds were investigated. The following conclusions were drawn from this study:

This is the accepted manuscript (postprint) of the following article:
M. Shahrouzifar, E. Salahinejad, E. Sharifi, *Co-incorporation of strontium and fluorine into diopside scaffolds: bioactivity, biodegradation and cytocompatibility evaluations*, Materials Science and Engineering: C, 103 (2019) 109752.
https://doi.org/10.1016/j.msec.2019.109752

a) Sr and F ions were successfully incorporated into diopside via the coprecipitation method used in this research.

b) The apatite-forming ability level of the samples was enhanced in the following order: undoped, co-doped, Sr-doped, and F-doped diopside.

c) A compromise between biodegradation and F incorporation into apatite was detected to explain the bioactivity difference of the samples.

d) Sr- and co-doped scaffolds exhibited the highest and lowest cell viability with respect to osteoblast-like MG-63 cells to 72 days of culture, respectively.

References

[1] C. Wu, J. Chang, W. Zhai, S. Ni, J. Wang, Porous akermanite scaffolds for bone tissue engineering: preparation, characterization, and in vitro studies, Journal of Biomedical Materials Research Part B: Applied Biomaterials, 78 (2006) 47-55.
[2] C. Wu, Y. Ramaswamy, H. Zreiqat, Porous diopside (CaMgSi2O6) scaffold: a promising bioactive material for bone tissue engineering, Acta biomaterialia, 6 (2010) 2237-2245.
[3] C. Wu, J. Chang, W. Zhai, S. Ni, A novel bioactive porous bredigite (Ca 7 MgSi 4 O 16) scaffold with biomimetic apatite layer for bone tissue engineering, Journal of Materials Science: Materials in Medicine, 18 (2007) 857-864.
[4] C. Wu, J. Chang, Degradation, bioactivity, and cytocompatibility of diopside, akermanite, and bredigite ceramics, Journal of Biomedical Materials Research Part B: Applied Biomaterials: An Official Journal of The Society for Biomaterials, The Japanese Society for Biomaterials, and The Australian Society for Biomaterials and the Korean Society for Biomaterials, 83 (2007) 153-160.
[5] Y. Huang, X. Jin, X. Zhang, H. Sun, J. Tu, T. Tang, J. Chang, K. Dai, In vitro and in vivo evaluation of akermanite bioceramics for bone regeneration, Biomaterials, 30 (2009) 5041-5048.
[6] T. Nonami, S. Tsutsumi, Study of diopside ceramics for biomaterials, Journal of Materials Science: Materials in Medicine, 10 (1999) 475-479.
[7] I. Kansal, A. Goel, D.U. Tulyaganov, M.J. Pascual, H.-Y. Lee, H.-W. Kim, J.M. Ferreira, Diopside (CaO· MgO· 2SiO 2)–fluorapatite (9CaO· 3P 2 O 5· CaF 2) glass-ceramics: Potential materials for bone tissue engineering, Journal of Materials Chemistry, 21 (2011) 16247-16256.
[8] O. Goudouri, E. Theodosoglou, E. Kontonasaki, J. Will, K. Chrissafis, P. Koidis, K. Paraskevopoulos, A. Boccaccini, Development of highly porous scaffolds based on bioactive silicates for dental tissue engineering, Materials Research Bulletin, 49 (2014) 399-404.
[9] H. Zreiqat, C. Howlett, A. Zannettino, P. Evans, G. Schulze-Tanzil, C. Knabe, M. Shakibaei, Mechanisms of magnesium-stimulated adhesion of osteoblastic cells to commonly used orthopaedic implants, Journal of Biomedical Materials Research Part A, 62 (2002) 175-184.

[10] M. Alcaide, P. Portoles, A. López-Noriega, D. Arcos, M. Vallet-Regí, M. Portoles, Interaction of an ordered mesoporous bioactive glass with osteoblasts, fibroblasts and lymphocytes, demonstrating its biocompatibility as a potential bone graft material, Acta biomaterialia, 6 (2010) 892-899.
[11] C. Wu, J. Chang, Degradation, bioactivity, and cytocompatibility of diopside, akermanite, and bredigite ceramics, Journal of Biomedical Materials Research Part B: Applied Biomaterials, 83 (2007) 153-160.
[12] S. Yamamoto, T. Nonami, H. Hase, N. Kawamura, Fundamental study on apatite precipitate ability of CaO-MgO-SiO 2 compounders employed pseudo body solution of application for biomaterials, Journal of the Australian Ceramic Society, 48 (2012) 180-184.
[13] T. Kobayashi, K. Okada, T. Kuroda, K. Sato, Osteogenic cell cytotoxicity and biomechanical strength of the new ceramic Diopside, Journal of Biomedical Materials Research: An Official Journal of The Society for Biomaterials and The Japanese Society for Biomaterials, 37 (1997) 100-107.
[14] Y. Miake, T. Yanagisawa, Y. Yajima, H. Noma, N. Yasui, T. Nonami, High-resolution and analytical electron microscopic studies of new crystals induced by a bioactive ceramic (diopside), Journal of dental research, 74 (1995) 1756-1763.
[15] N.Y. Iwata, G.-H. Lee, Y. Tokuoka, N. Kawashima, Sintering behavior and apatite formation of diopside prepared by coprecipitation process, colloids and surfaces B: Biointerfaces, 34 (2004) 239-245.
[16] W. Zhai, H. Lu, C. Wu, L. Chen, X. Lin, K. Naoki, G. Chen, J. Chang, Stimulatory effects of the ionic products from Ca–Mg–Si bioceramics on both osteogenesis and angiogenesis in vitro, Acta biomaterialia, 9 (2013) 8004-8014.
[17] D. Sriranganathan, N. Kanwal, K.A. Hing, R.G. Hill, Strontium substituted bioactive glasses for tissue engineered scaffolds: the importance of octacalcium phosphate, Journal of Materials Science: Materials in Medicine, 27 (2016) 39.
[18] C. Wu, Y. Ramaswamy, D. Kwik, H. Zreiqat, The effect of strontium incorporation into CaSiO3 ceramics on their physical and biological properties, Biomaterials, 28 (2007) 3171-3181.
[19] A. Goel, R.R. Rajagopal, J.M. Ferreira, Influence of strontium on structure, sintering and biodegradation behaviour of CaO–MgO–SrO–SiO2–P2O5–CaF2 glasses, Acta Biomaterialia, 7 (2011) 4071-4080.
[20] J. Lao, J.-M. Nedelec, E. Jallot, New strontium-based bioactive glasses: physicochemical reactivity and delivering capability of biologically active dissolution products, Journal of Materials Chemistry, 19 (2009) 2940-2949.
[21] Y. Zhu, M. Zhu, X. He, J. Zhang, C. Tao, Substitutions of strontium in mesoporous calcium silicate and their physicochemical and biological properties, Acta biomaterialia, 9 (2013) 6723-6731.
[22] N. Esmati, T. Khodaei, E. Salahinejad, E. Sharifi, Fluoride doping into SiO2-MgO-CaO bioactive glass nanoparticles: bioactivity, biodegradation and biocompatibility assessments, Ceramics International, 44 (2018) 17506-17513.
[23] M.J. Baghjeghaz, E. Salahinejad, Enhanced sinterability and in vitro bioactivity of diopside through fluoride doping, Ceramics International, 43 (2017) 4680-4686.
[24] E. Salahinejad, M.J. Baghjeghaz, Structure, biomineralization and biodegradation of Ca-Mg oxyfluorosilicates synthesized by inorganic salt coprecipitation, Ceramics International, 43 (2017) 10299-10306.
[25] M. Shahrouzifar, E. Salahinejad, Strontium doping into diopside tissue engineering scaffolds, Ceramics International, 45 (2019) 10176–10181.
[26] N.O. Engin, A.C. Tas, Manufacture of macroporous calcium hydroxyapatite bioceramics, Journal of the European Ceramic Society, 19 (1999) 2569-2572.

This is the accepted manuscript (postprint) of the following article:
M. Shahrouzifar, E. Salahinejad, E. Sharifi, *Co-incorporation of strontium and fluorine into diopside scaffolds: bioactivity, biodegradation and cytocompatibility evaluations*, Materials Science and Engineering: C, 103 (2019) 109752.
https://doi.org/10.1016/j.msec.2019.109752

[27] A. Buzatu, N. Buzgar, The Raman study of single-chain silicates, Analele Stiintifice de Universitatii Al Cuza din Iasi. Sect. 2, Geologie, 56 (2010) 107.
[28] H. Aguiar, J. Serra, P. González, B. León, Structural study of sol–gel silicate glasses by IR and Raman spectroscopies, Journal of Non-Crystalline Solids, 355 (2009) 475-480.
[29] E. Huang, C. Chen, T. Huang, E. Lin, J.-a. Xu, Raman spectroscopic characteristics of Mg-Fe-Ca pyroxenes, American Mineralogist, 85 (2000) 473-479.
[30] P. Richet, B.O. Mysen, J. Ingrin, High-temperature X-ray diffraction and Raman spectroscopy of diopside and pseudowollastonite, Physics and Chemistry of Minerals, 25 (1998) 401-414.
[31] M.C. Domeneghetti, G.M. Molin, V. Tazzoli, Crystal-chemical implications of the Mg (super 2+)-Fe (super 2+) distribution in orthopyroxenes, American Mineralogist, 70 (1985) 987-995.
[32] M. Cameron, J. Papike, Structural and chemical variations in pyroxenes, American Mineralogist, 66 (1981) 1-50.
[33] V. Dimitrov, S. Sakka, Electronic oxide polarizability and optical basicity of simple oxides. I, Journal of Applied Physics, 79 (1996) 1736-1740.
[34] J. Etchepare, Study by Raman spectroscopy of crystalline and glassy diopside, Amorphous materials, 337 (1972).
[35] C.J. Brinker, G.W. Scherer, Sol-gel science: the physics and chemistry of sol-gel processing, Academic press2013.
[36] E. Bernstein, G. Meredith, Raman spectra of SiF4 and GeF4 crystals, The Journal of Chemical Physics, 67 (1977) 4132-4138.
[37] N. OKII, S. NISHIMURA, K. KURISU, Y. TAKESHIMA, T. UOZUMI, In vivo histological changes occurring in hydroxyapatite cranial reconstruction, Neurologia medico-chirurgica, 41 (2001) 100-104.
[38] T. Freyman, I. Yannas, L. Gibson, Cellular materials as porous scaffolds for tissue engineering, Progress in Materials Science, 46 (2001) 273-282.
[39] G. Sauer, W. Zunic, J. Durig, R. Wuthier, Fourier transform Raman spectroscopy of synthetic and biological calcium phosphates, Calcified tissue international, 54 (1994) 414-420.
[40] H. Tsuda, J. Arends, Raman spectra of human dental calculus, Journal of dental research, 72 (1993) 1609-1613.
[41] A. Antonakos, E. Liarokapis, T. Leventouri, Micro-Raman and FTIR studies of synthetic and natural apatites, Biomaterials, 28 (2007) 3043-3054.
[42] Y.C. Fredholm, N. Karpukhina, D.S. Brauer, J.R. Jones, R.V. Law, R.G. Hill, Influence of strontium for calcium substitution in bioactive glasses on degradation, ion release and apatite formation, Journal of The Royal Society Interface, 9 (2012) 880-889.
[43] P. De Aza, F. Guitian, C. Santos, S. De Aza, R. Cusco, L. Artus, Vibrational properties of calcium phosphate compounds. 2. Comparison between hydroxyapatite and β-tricalcium phosphate, Chemistry of Materials, 9 (1997) 916-922.
[44] B.O. Fowler, M. Markovic, W.E. Brown, Octacalcium phosphate. 3. Infrared and Raman vibrational spectra, Chemistry of Materials, 5 (1993) 1417-1423.
[45] D. Nelson, B. Williamson, Raman spectra of phosphate and monofluorophosphate ions in several dentally-relevant materials, Caries research, 19 (1985) 113-121.
[46] F.A. Shah, D.S. Brauer, N. Desai, R.G. Hill, K.A. Hing, Fluoride-containing bioactive glasses and Bioglass® 45S5 form apatite in low pH cell culture medium, Materials Letters, 119 (2014) 96-99.
[47] C. Wu, W. Fan, M. Gelinsky, Y. Xiao, P. Simon, R. Schulze, T. Doert, Y. Luo, G. Cuniberti, Bioactive SrO–SiO2 glass with well-ordered mesopores: characterization, physiochemistry and biological properties, Acta Biomaterialia, 7 (2011) 1797-1806.

This is the accepted manuscript (postprint) of the following article:
M. Shahrouzifar, E. Salahinejad, E. Sharifi, *Co-incorporation of strontium and fluorine into diopside scaffolds: bioactivity, biodegradation and cytocompatibility evaluations*, Materials Science and Engineering: C, 103 (2019) 109752.
https://doi.org/10.1016/j.msec.2019.109752

[48] H. Zreiqat, Y. Ramaswamy, C. Wu, A. Paschalidis, Z. Lu, B. James, O. Birke, M. McDonald, D. Little, C.R. Dunstan, The incorporation of strontium and zinc into a calcium–silicon ceramic for bone tissue engineering, Biomaterials, 31 (2010) 3175-3184.
[49] D.S. Brauer, N. Karpukhina, M.D. O'Donnell, R.V. Law, R.G. Hill, Fluoride-containing bioactive glasses: effect of glass design and structure on degradation, pH and apatite formation in simulated body fluid, Acta Biomaterialia, 6 (2010) 3275-3282.
[50] G. Lusvardi, G. Malavasi, L. Menabue, V. Aina, C. Morterra, Fluoride-containing bioactive glasses: surface reactivity in simulated body fluids solutions, Acta Biomaterialia, 5 (2009) 3548-3562.
[51] Y. Chen, X. Miao, Thermal and chemical stability of fluorohydroxyapatite ceramics with different fluorine contents, Biomaterials, 26 (2005) 1205-1210.
[52] P. Taddei, E. Modena, A. Tinti, F. Siboni, C. Prati, M.G. Gandolfi, Effect of the fluoride content on the bioactivity of calcium silicate-based endodontic cements, Ceramics International, 40 (2014) 4095-4107.
[53] C. Ohtsuki, T. Kokubo, T. Yamamuro, Mechanism of apatite formation on CaOSiO2P2O5 glasses in a simulated body fluid, Journal of Non-Crystalline Solids, 143 (1992) 84-92.
[54] M. Diba, F. Tapia, A.R. Boccaccini, L.A. Strobel, Magnesium-containing bioactive glasses for biomedical applications, International Journal of Applied Glass Science, 3 (2012) 221-253.
[55] E. Gentleman, Y.C. Fredholm, G. Jell, N. Lotfibakhshaiesh, M.D. O'Donnell, R.G. Hill, M.M. Stevens, The effects of strontium-substituted bioactive glasses on osteoblasts and osteoclasts in vitro, Biomaterials, 31 (2010) 3949-3956.
[56] S. Hesaraki, M. Alizadeh, H. Nazarian, D. Sharifi, Physico-chemical and in vitro biological evaluation of strontium/calcium silicophosphate glass, Journal of Materials Science: Materials in Medicine, 21 (2010) 695-705.
[57] D. Boyd, G. Carroll, M. Towler, C. Freeman, P. Farthing, I. Brook, Preliminary investigation of novel bone graft substitutes based on strontium–calcium–zinc–silicate glasses, Journal of Materials Science: Materials in Medicine, 20 (2009) 413-420.
[58] K. Qiu, X.J. Zhao, C.X. Wan, C.S. Zhao, Y.W. Chen, Effect of strontium ions on the growth of ROS17/2.8 cells on porous calcium polyphosphate scaffolds, Biomaterials, 27 (2006) 1277-1286.
[59] C. Wu, Y. Zhou, C. Lin, J. Chang, Y. Xiao, Strontium-containing mesoporous bioactive glass scaffolds with improved osteogenic/cementogenic differentiation of periodontal ligament cells for periodontal tissue engineering, Acta Biomaterialia, 8 (2012) 3805-3815.
[60] J. Isaac, J. Nohra, J. Lao, E. Jallot, J.-M. Nedelec, A. Berdal, J.-M. Sautier, Effects of strontium-doped bioactive glass on the differentiation of cultured osteogenic cells, Eur Cell Mater, 21 (2011) 130-143.

This is the accepted manuscript (postprint) of the following article:
M. Shahrouzifar, E. Salahinejad, E. Sharifi, *Co-incorporation of strontium and fluorine into diopside scaffolds: bioactivity, biodegradation and cytocompatibility evaluations*, Materials Science and Engineering: C, 103 (2019) 109752.
https://doi.org/10.1016/j.msec.2019.109752

Figures

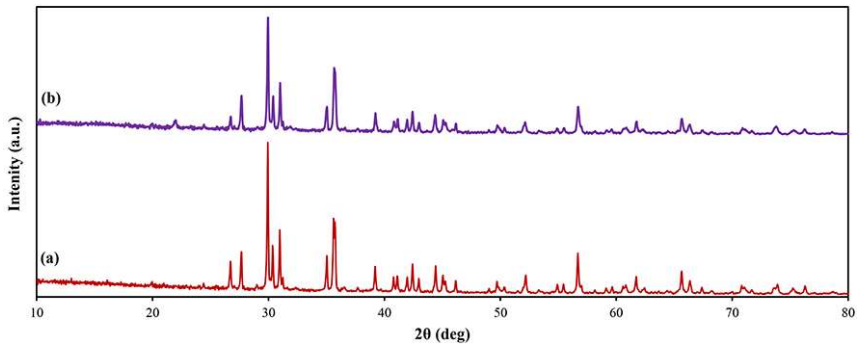

Fig. 1. XRD patterns of the F-doped (c), and co-doped (d) samples. All peaks are assigned to diopside.

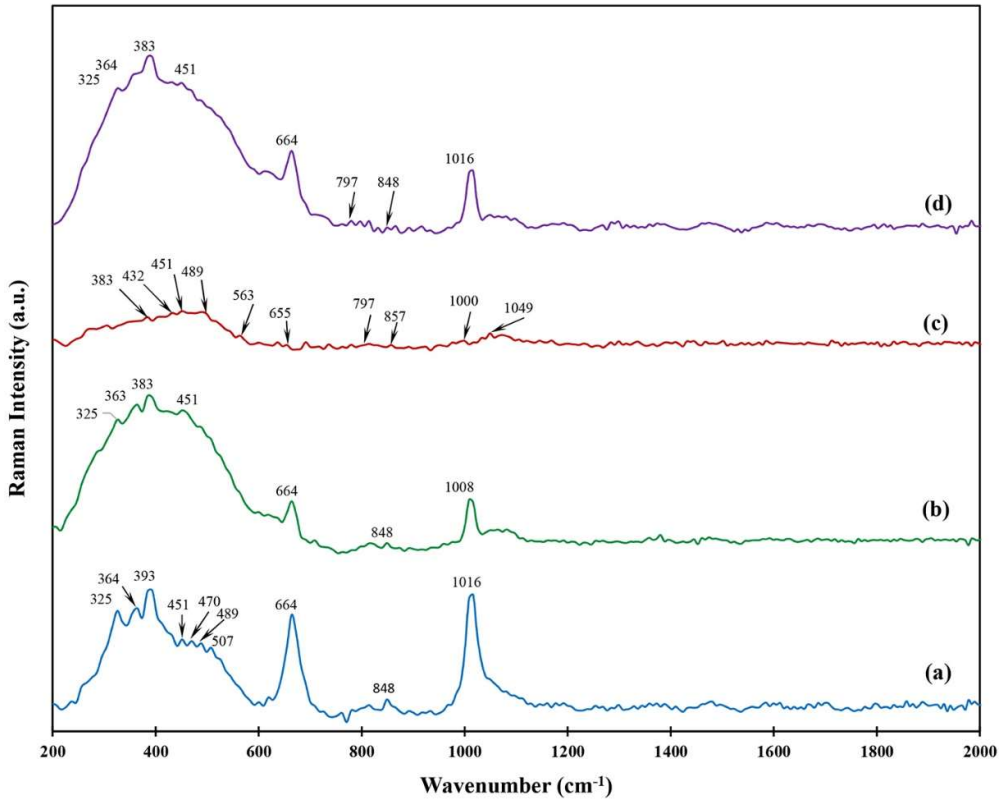

Fig. 2. Raman spectra of the pure (a), Sr-doped (b), F-doped (c), and co-doped (d) diopside scaffolds after sintering.

This is the accepted manuscript (postprint) of the following article:
M. Shahrouzifar, E. Salahinejad, E. Sharifi, *Co-incorporation of strontium and fluorine into diopside scaffolds: bioactivity, biodegradation and cytocompatibility evaluations*, Materials Science and Engineering: C, 103 (2019) 109752.
https://doi.org/10.1016/j.msec.2019.109752

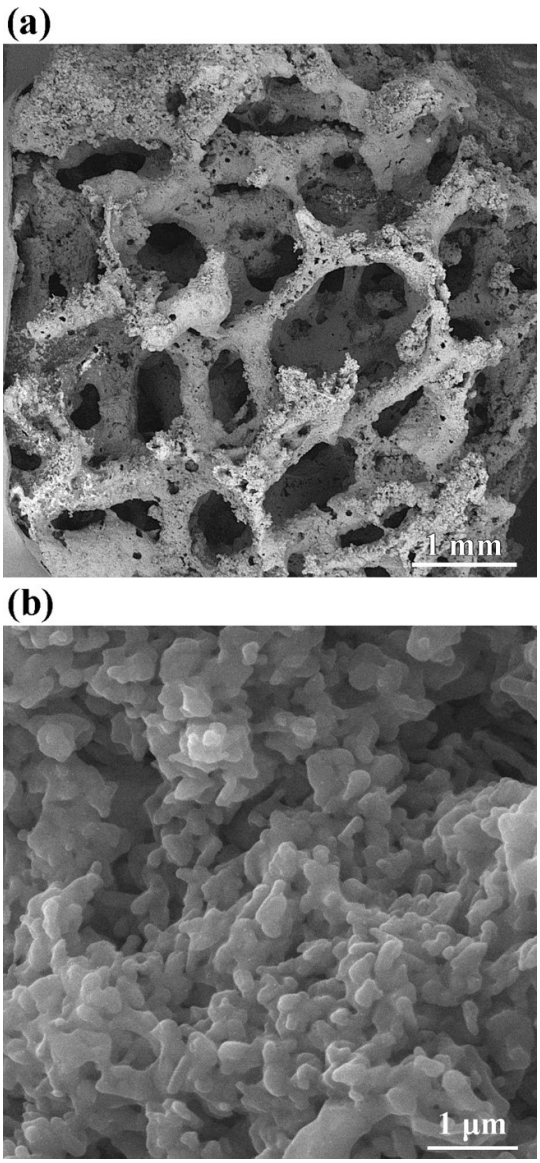

Fig. 3. FESEM micrographs of the pure diopside scaffold in two magnifications (a, b).

This is the accepted manuscript (postprint) of the following article:
M. Shahrouzifar, E. Salahinejad, E. Sharifi, *Co-incorporation of strontium and fluorine into diopside scaffolds: bioactivity, biodegradation and cytocompatibility evaluations*, Materials Science and Engineering: C, 103 (2019) 109752.
https://doi.org/10.1016/j.msec.2019.109752

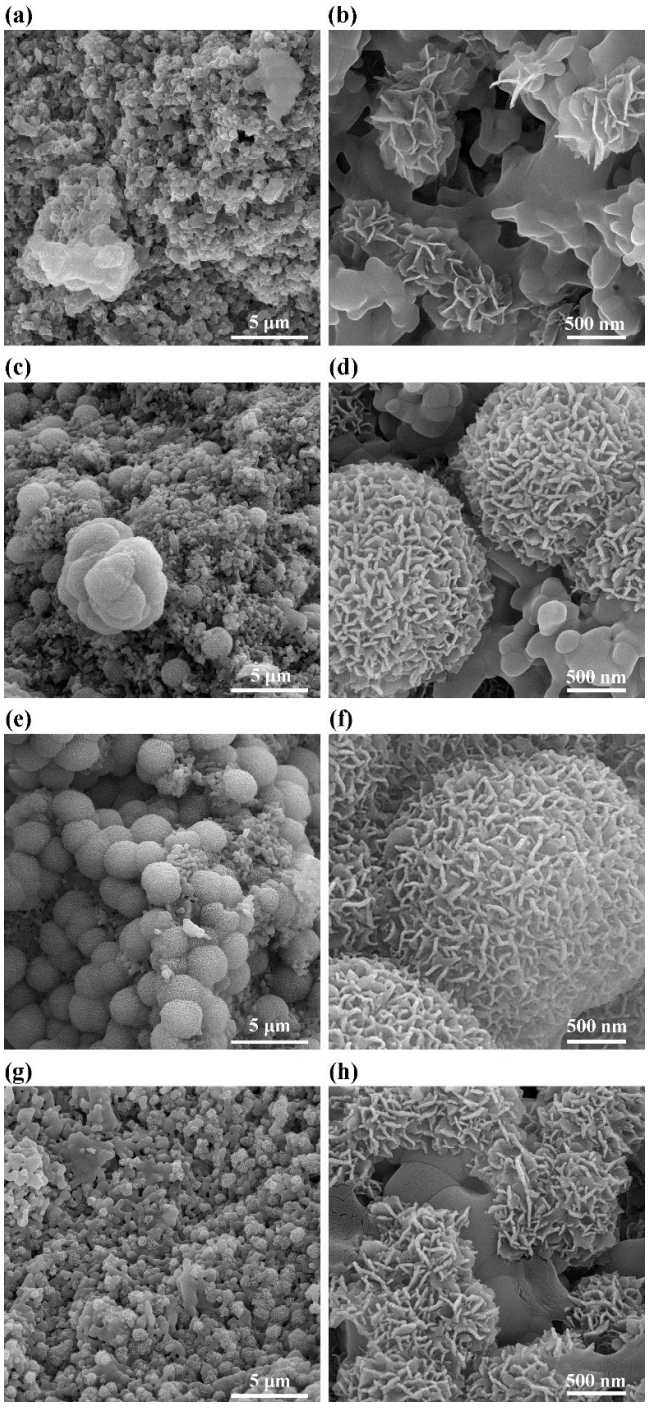

Fig. 4. Low- and high-magnification FESEM micrographs of the pure (a, b), Sr-doped (c, d), F-doped (e, f), and co-doped (g, h) diopside scaffolds after soaking in the SBF for 7 days.

This is the accepted manuscript (postprint) of the following article:
M. Shahrouzifar, E. Salahinejad, E. Sharifi, *Co-incorporation of strontium and fluorine into diopside scaffolds: bioactivity, biodegradation and cytocompatibility evaluations*, Materials Science and Engineering: C, 103 (2019) 109752.
https://doi.org/10.1016/j.msec.2019.109752

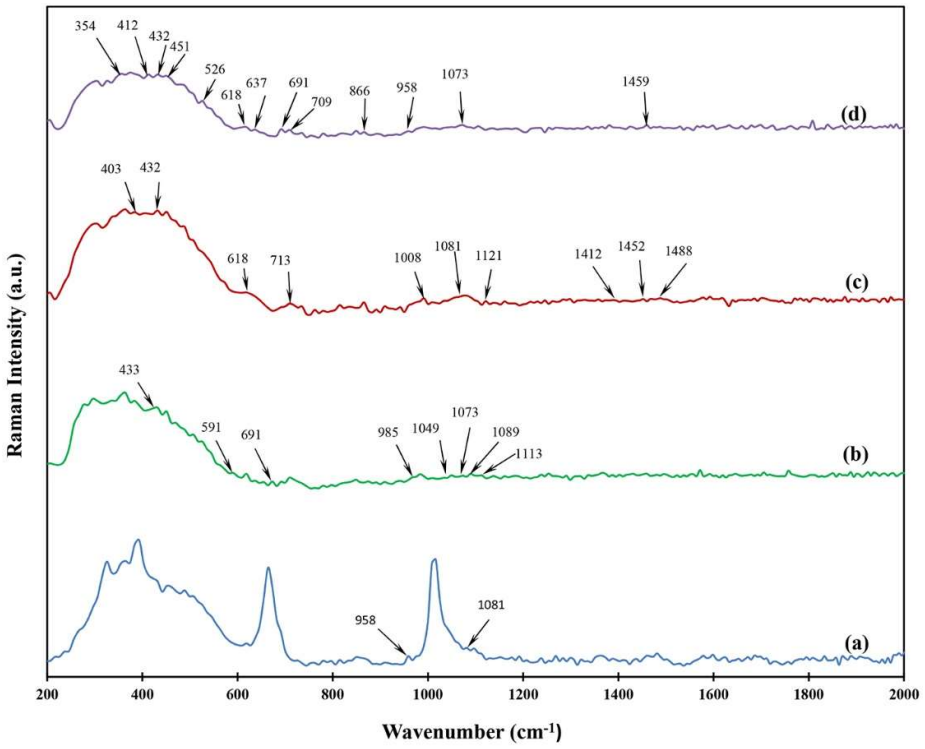

Fig. 5. Raman spectra of the pure (a), Sr-doped (b), F-doped (c), and co-doped (d) diopside scaffolds after soaking in the SBF for 7 days.

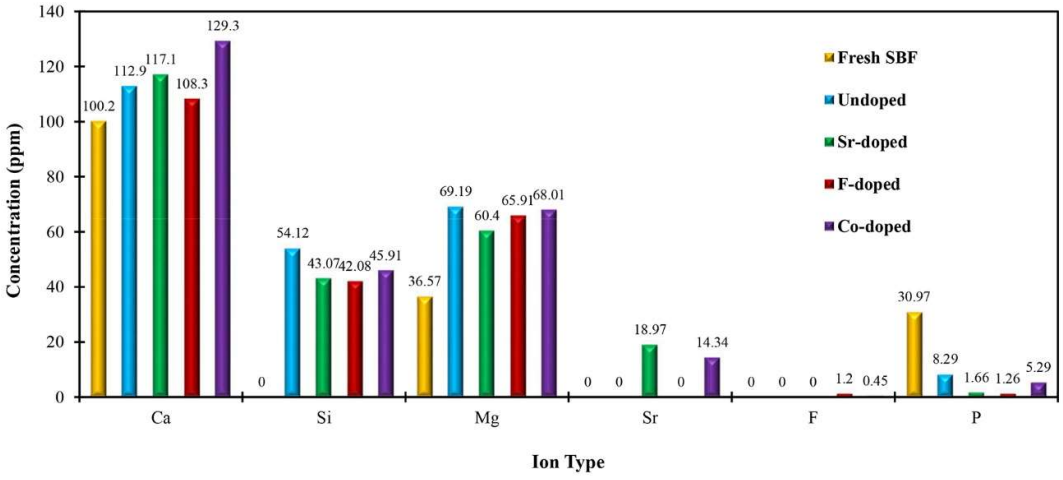

Fig. 6. ICP results on the SBF after 7 days of contact with the scaffolds.

This is the accepted manuscript (postprint) of the following article:
M. Shahrouzifar, E. Salahinejad, E. Sharifi, *Co-incorporation of strontium and fluorine into diopside scaffolds: bioactivity, biodegradation and cytocompatibility evaluations*, Materials Science and Engineering: C, 103 (2019) 109752.
https://doi.org/10.1016/j.msec.2019.109752

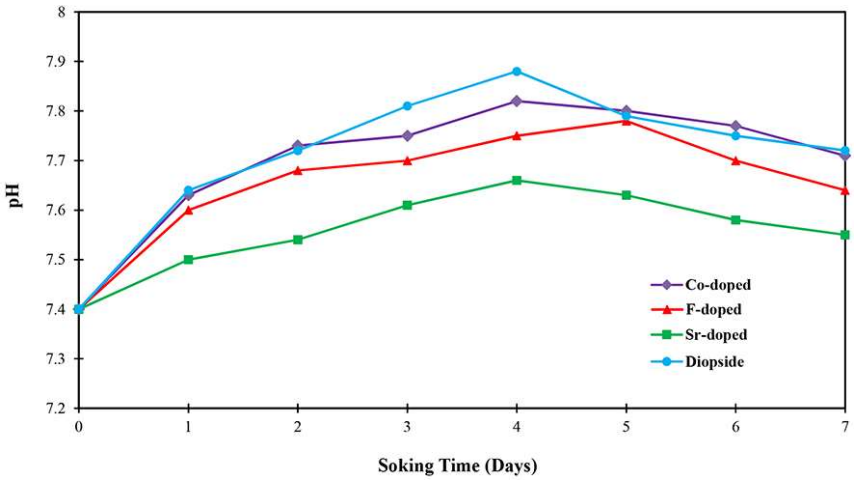

Fig. 7. pH variation of the SBF in contact with scaffolds.

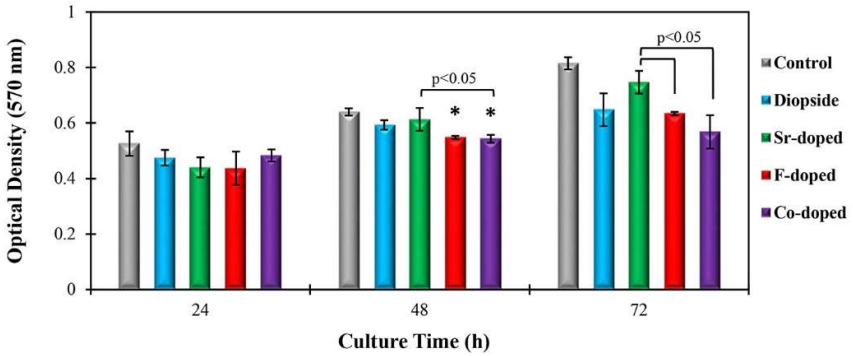

Fig. 8. MTT results on the cell cultures. The scaffold-free culture medium was used as the control. P<0.05 was considered as the significance level. * indicates the significant difference with respect to the undoped sample.